SUPPLEMENTAL MATERIAL

Arp2/3 complex is critical for lamellipodia and organization of cell-matrix adhesion but dispensable for fibroblast chemotaxis

Wu et al.

EXTENDED EXPERIMENTAL PROCEDURES

Reagents and Materials: Commercial antibodies were obtained from Cell Signaling Technologies (Akt (pan), Phosphor-Akt(Ser473), ECM Bioscience (Arp2(C-terminal region)), Sigma-Aldrich (Monoclonal anti-vinculin Clone hVIN-1, Monoclonal anti-ARP3, CloneFMS338), Upstate Biotechnology (Anti-FAK clone 4.47, Rabbit (Polyclonal) Anti-FAK[pY397]), BD Biosciences (Mouse anti-Paxillin), Millipore(Anti-p34-Arc/ARPC2), and Ambion Applied Biosystems (Anti-GAPDH). AlexaFluor647 dye conjugated phalloidin was from Invitrogen. Arp2/3 complex inhibitor CK-666 and the inactive control CK-689 are from EMD4Biosciences. Latrunculin B, (-)-Blebbistatin, Laminin were from Sigma-Aldrich, human plasma Fibronectin from BD Biosciences, Human Vitronectin from R & D Systems, Cy5 labeling kit from Amersham, Rhodamine Red-X and HRP conjugated secondary antibodies were from Jackson ImmunoResearch Laboratories. Bovine Arp2/3 complex was from Cytoskeleton Inc. PLL(20)-g[3.5]-PEG(2) was from SuSoS (Dübendorf, Switzerland). Western blotting was done by standard techniques. For quantitative western analysis, the blot was probed using primary antibodies followed by incubation with infrared-conjugated secondary antibodies. The membrane was scanned in an Odyssey SA scanner (LI-COR Biosciences, Lincoln, NE), and band intensities were quantified using the Odyssey software. Molecular cloning was conducted using standard procedures and details including primer sequences are available upon request.

Cell culture, viral transduction and generation of 2xKD cells: Cells were cultured in DMEM supplemented with 10% FBS (HyClone), 100 U/mL penicillin, 100 µg/mL streptomycin and 292 µg/mL L-glutamine. DMEM supplemented with 0.1% fatty-acid free BSA (Equitech-Bio), 100 U/mL penicillin, 100 µg/mL streptomycin and 292 µg/mL L-glutamine was used to culture cells during serum starvation. Transient transfections were performed using FuGene 6 (Roche) for HEK293 FT cells. Retroviral packaging, infections, and fluorescence-activated cell sorting were as described (Bear et al., 2000). Lentivirus production and infection were as described (Cai et al., 2007).

IA32 cells infected with shArp2-mChry (target sequence: TGACCATGGCTTTAAACA AGTT) and shp34-EGFP (from (Cai et al., 2008)) viruses were cloned by fluorescence-activated cell-sorting (FACS) and screened for p34 and Arp2 expressions by Western blot. Infection with adenoviruses expressing Cre-recombinase (U of Iowa Gene Transfer Core) was used to deplete fluorescent protein expression before a second round of FAC sorting to yield 2xKD cells.

Growth Curves: MEFs were plated at 1×10^4 cells/well as triplicates in 24 well plates. Cell number was counted every 24 hr for indicated days, and normalized to the number

on the first day. Growth curve was measured the same way for IA32 NS and 2xKD cells, but with different initial cell number (3000 cells/well). Cell viability was determined by trypan blue exclusion.

Microinjection Rescue of 2xKD cells: Bovine Arp2/3 protein complex was reconstituted with distilled water to 5 mg/mL in the following buffer: 20 mM Tris pH 7.5, 25 mM KCl, 1 mM $MgCl_2$, 0.5 mM EDTA, 0.1 mM ATP, 0.2% dextran and 2% sucrose. To confirm successful microinjection, rhodamine-dextran was co-loaded with the Arp2/3 complex. Microinjection of Arp2/3 complex was performed with a semiautomatic Eppendorf InjectMan NI 2/Femtojet system. Injected volume was estimated to be less than 10% total cell volume.

Spreading assay: Cell spreading assays were performed as described previously (Isaji et al., 2009) with minor modifications. Briefly, NS and 2xKD cells were serum starved for 1 hr. Cells were then detached with trypsin containing 1 mM EDTA, washed with regular cell culture medium, and then suspended at 1×10^4 cells/mL. Cells were seeded at 1000 cells/well in the electrode sensors (16X E-plate 16, Roche) coated with 25 µg/mL FN. Cell adhesion during the subsequent 5 hr period was continually monitored by taking a measurement with the RTCA apparatus (Roche Applied Science) operated with RTCA Software every 30 sec.

Phase contrast microscopy of cell spreading: Cells were trypsinized, resuspended in complete culture medium. Phase contrast time-lapse sequential cell images were captured with Nikon BioStation IM.

Light Microscopy and image analysis

Immunofluorescence: For immunofluorescent staining, the cells were fixed, stained and mounted as described previously (Bear et al., 2002). Cells were plated on acid-washed coverslips coated with 10 µg/mL FN overnight before fixing with 4% PFA and permeabilized in 0.1% Triton X-100 in PBS for 5 min. Cells were then blocked for 15 min in PBS containing 5% normal goat serum (Jackson Laboratories) and 5% fatty-acid-free BSA. Primary antibodies were applied to cells in PBS containing 1% BSA for 1 hr at room temperature. Cells were stained in various combinations with AlexaFluor-647 phalloidin for F-actin (1:200 dilution), p34Arc (1:250 dilution), Pax (1:500 dilution), Vin (1:400 dilution) or FAK (1:400 dilution) antibodies. After washing the cells three times in PBS, fluorescent dye conjugated secondary antibodies were diluted to 1:250 in 1% BSA in PBS and applied to the coverslips for 1 hr. After three washes in PBS, the coverslips were mounted onto slides with Fluoromount G (Electron Microscopy Sciences).

Images were captured using a FluoView FV1000 scanning confocal inverted microscope (FV1000, Olympus) equipped with a 1.42 N.A. 60× objective, a Hamamatsu PMT and controlled by Fluoview software. Maximum intensity projection was generated with ImageJ (ZProject-Maximum intensity function) from a z-stack (4 slices, 100 nm interval). Images were combined and annotated in Photoshop for presentation. Images

were initially saved as 16-bit tiff files and converted to 8-bit tiff files in ImageJ during the analysis.

Single cell tracking: Cells were plated on 10 µg/mL FN-coated glass bottom culture dishes (MatTek Corporation) for 8-12 hr before imaging. Time-lapse microscopy was performed on an Olympus VivaView FL incubator fluorescent microscope (20x objective) with a Hamamatsu camera (OrcaERAG - c4742-80-12AG), or with Nikon BioStation IM (20x objective). Cell speed was measured with ImageJ using the Manual Tracking plug-in (http://rsbweb.nih.gov/ij/plugins/track/track.html).

In ECM biphasic response experiments, glass bottom culture dishes (MatTek Corporation) dishes were first coated with indicated concentrations of FN at 37 °C for 1 hr and thoroughly washed with distilled water. Coated dishes were then blocked with 1 mg/mL PLL(20)-g[3.5]-PEG(2) at 37 °C for 1 hr to prevent non-specific cell adhesion.

Focal adhesion imaging: IA32 cells infected with shNS-GFP-PAX, shNS-Vin-GFP, mChry-FAK, 2xKD cells infected with shArp2-GFP-PAX, shArp2-Vin-GFP, mChry-FAK, and Rat2 cells treated with CK-666 or CK-689 were plated on FN coated Delta T dishes (Bioptechs). Total internal reflectance microscopy was performed using Olympus cell^TIRF illuminator motorized multicolor TIRF microscope (60x objective). Images were captured using an ImagEM camera (c9100-14). Images were taken every 15 sec for 1 hr to monitor focal adhesion dynamics and 150 sec for 3 hr to analyze focal adhesion alignment.

Electron Microscopy

Scanning EM: Cells were plated onto 10 µg/mL FN coated coverslips overnight, rinsed gently 2-3 times with serum-free medium warmed to 37 °C and fixed with 3% glutarldehyde in 0.1 M sodium cacodylate buffer (pH 7.4) with 0.05% $CaCl_2$ for 30min at room temperature followed by subsequent treatment with 2% tannic acid for 10 min and 1% osmium tetroxide in water for 10 min (Katsumoto et al., 1981). The coverslips were dehydrated with ethanol and dried in a Samdri-795 critical point dryer using carbon dioxide as the transitional solvent (Tousimis Research Corporation, Rockville, MD). Coverslips were mounted on aluminum planchets with double-sided carbon adhesive and coated with 10 nm of gold-palladium alloy (60Au:40Pd, Hummer X Sputter Coater, Anatech USA, Union City, CA). Images were taken using a Zeiss Supra 25 FESEM operating at 5 kV, working distance of 5mm, and 10µm aperture (Carl Zeiss SMT Inc., Peabody, MA).

Cryo-shadowing EM: Nickel grids (150-mesh) covered with a carbon film were treated with a glow discharge at 200 torr for 2 min. FN (10 µg/mL) was used to coat the glow-treated surface for 1 hr at 37 °C. Cells were plated on grids for 2.5 hr in regular cell culture medium before extraction with extraction buffer (1% Triton X-100 and 2 µM phalloidin in PEM buffer containing 100 mM PIPES, 1 mM EGTA, 1mM $MgCl_2$, pH 6.9) for 4 min at room temperature (Svitkina, 2005). After extraction, cells were rinsed with PEM buffer (pH 6.9) for 1 min and fixed with 1% glutaraldehyde in PBS for 5 min at room temperature. After fixation, grids were briefly rinsed with distilled water and transferred to the chamber of an FEI Vitrobot freezing robot held at 37 °C and 100%

humidity (Ozgur et al., 2011). The water remaining on the grid was gently blotted with filter paper before plunging the grid into liquid ethane for rapid freezing. The grids in an enclosed box under liquid nitrogen were transferred to the stage of a modified Balzers freeze etch machine held at -120 °C. The chamber was evacuated and the sample slowly freeze dried at $1x10^{-5}$ to $5x10^{-7}$ torr for 4 hr while the temperature was ramped from -120 to -85 °C. The samples were then rotary shadowcast with tungsten prior to breaking the vacuum.

The grids were examined in an FEI Tecnai T12 Teat 80 kV. The images were taken with either sheet film or using a GATAN Inc Oris 1000 2Kx2K digital camera. Images on film were scanned using an Imacon 848 film scanner. Image levels were adjusted and the contrast inverted using Adobe Photoshop.

Directional migration assays

Microfludic device preparation: Transparency masks were printed using a high-resolution printer (Fineline Imaging, CO). The pattern for the chemotaxis chamber was fabricated on 4" silicon wafers using a two-step photolithography process. The first step involved a 5 µm tall layer of SU-8 (25) from microposit and the microcapillaries were transferred to the wafer. After developing the first layer a second 100 µm tall layer of SU-8 (100) was applied to the same wafer and after alignment the channels were transferred to the wafer. After developing and post-baking, the silicon wafer was exposed to silane overnight. Polymethylsiloxane (PDMS) was then poured on the wafer and cured in overnight at 70ºC. Individual PDMS devices were cut out from the wafer and placed in a clean dish until use. The sharp ends of 20 gauge needles were cut off and the ends were then smoothed using a Dremel tool. The needles were then used to punch out ports in the devices. The devices were then washed with water and ethanol, blow-dried and exposed to air plasma for 2 min in a plasma cleaner (Harrick plasma). Glass bottom culture dishes (MatTek) or Delta T dishes (Bioptechs) glass dishes were cleaned using water and ethanol and then exposed to plasma for 2 min. The PDMS device was placed into contact with glass dish bottom immediately following plasma treatment of both pieces, ensuring that an irreversible seal was formed. The cell culture chamber was then filled with 10 µg/mL FN for 1 hr at 37 ºC, followed by flushing with sterile PBS. Cells were loaded into the cell culture chamber using a gel loading pipette tip. The cell chamber ports were plugged with short pieces of tubing (Upchurch Scientific, .0025" x 1/32").

Chemotactic gradients: The exit ports of the sink and source channels were connected to waste using tubing of ID 0.015". Gas tight 100 µL Hamilton glass syringes (81020,1710TLL 100 µL SYR) were connected to 27 1/2 gauge needles connected to tubing. The source syringe and tubing were filled serum free DMEM containing indicated chemoattractant and 10 µg/mL of TRITC-dextran to visualize the gradient. The sink syringe and tubing were filled with serum free DMEM. The tubing was then inserted into the source and sink channels respectively, and the syringe pump was operated at a flow rate of 20 nL/min. A stable gradient was then established in the cell culture chamber within 30 min, and typically remained stable for 18 hr as monitored by TRITC-dextran fluorescent intensity.

Haptotaxis gradients: Identical chambers as in the chemotaxis experiments were prepared. After bonding device to dish, the cell culture was coated with a minimal concentration of 2.5 µg/mL FN (or 5 µg/mL LN) to promote cell attachment throughout the chamber. The source and sink syringes were filled with the indicated concentration FN (or LN or VTN) in PBS or PBS alone respectively. The syringe pump was maintained at a flow rate of 20 nL/min. The chambers were allowed to equilibrate for 1 hr. Once the ECM gradient was established, 1 mg/mL PLL(20)-g[3.5]-PEG(2) was flowed into all channels of the device to block non-specific adhesion. Thorough wash of the chambers with distilled water was performed before plating the cells.

Directional migration image acquisition and analysis: Chemotaxis assays were performed on an Olympus DSU microscope with a 20X objective using MetaMorph imaging software. Images were collected every 10 min for over 12 hr. Haptotaxis assays were performed on the Nikon Biostation IM using a 20x objective and at the same time interval. Individual cells were manually tracked using ImageJ software Manual Tracking plug-in. The tracks obtained were further analyzed using the chemotaxis tool developed by IBIDI (http://www.ibidi.de/applications/ap_chemotaxis.html#imageanalysis). This analysis tool was used to extract the FMI and histogram of angular direction of tracks from the manual tracking results. To obtain the Compass Parameter (CP), the histograms obtained were further analyzed in GraphPad Prism software by performing a non linear curve fit to the chemotaxis equation.

Focal Adhesion Segmentation and Measurements: To identify focal adhesions in each image of a time-lapse series, a set of segmentation methods were used (Berginski et al., 2011). Each movie was cropped to only include one cell. Starting with the raw images from the TIRF movies (Fig. S4A), we used a high-pass filter to minimize background noise (Fig. S4B) and the overall distribution of pixel intensities after high-pass filtering (Fig. S4C) was used to select a threshold for adhesion detection. For all image sets examined, we selected a threshold of the mean plus two standard deviations of the high-pass filtered pixel intensities. We then applied the threshold and connected components labeling to identify each adhesion and removed any single pixel objects identified (Figure S4D). After identifying the adhesions, they were tracked through time using a previously published method (Berginski et al., 2011) and a range of properties were collected (Fig. 6D). All of the per adhesion properties (mean area, axial ratio, major axis length, minor access length and longevity) were only calculated for adhesions where both a birth and death event was detected.

In order to measure the global alignment of focal adhesions across the entire cell, we developed the focal adhesion alignment index (FAAI, Figure S5A, B). The index is determined by a two-step process. The first step involved collecting and filtering the adhesion angles in each image of the time-lapse, while the second step involved searching for a reference angle that minimizes the deviation between all of the adhesion angle measurements. We began the first step by segmenting the adhesions from each frame of a time-lapse movie. From this set of identified adhesions in each frame, we calculated the best-fit ellipse to each adhesion (Figure S5A). From this ellipse, we found the length of the major axis, the length of the minor axis and the angle the major axis of the adhesion made with the positive x-axis. Angle measurement was on a scale of -90°-

90° to avoid the ambiguity of the 360° measurement scale (Figure S5A). We set the minimum ratio of the lengths of the major over minor axes to three as a filter to select adhesions whose orientation could be determined (Figure S5A). After collecting the adhesion angles with the positive x-axis as the reference, the second step of calculating the index began with a search through a range of potential reference angles. The search began at with the x-axis as the 0° position and the calculation of the standard deviation of the adhesion angles (Figure S5B column 1). Then the reference angle is increased by 0.1°, the adhesion angles with the new reference axis are recalculated and the standard deviation measured. This search process continued until the full range (0°-179.9°) of potential reference angles had been sampled (see intermediate reference angles in Figure S5B columns 2-4). The FAAI is calculated for all reference angles as:

FAAI = 90 – SD (adhesion angles at a given reference angle)

We choose this formulation as it provides an intuitive interpretation of the index; high values of the FAAI indicate that the adhesions in a cell are well aligned (low standard deviation) and low values of the FAAI indicate that the adhesions are not well aligned (high standard deviation). The dominant adhesion angle is defined as the reference angle that maximizes the FAAI. In cases where there are multiple angles that maximize the FAAI, the reference angle that minimizes the absolute value of the mean adhesion angle is selected from the list of angles that maximize the FAAI as the dominant angle. The final number reported is the value of the FAAI at the dominant angle.

We also wanted to measure the variation through time in the angles formed by single adhesions. To measure single adhesion angle variation, we tracked the adhesions identified through each frame of the movie using a tracking method based on overlap with prior adhesions and the centroid distance between nearby adhesions (Berginski et al., 2011). From this data set of tracked adhesions we excluded angle measurements with a major/minor length ratio less than three and determined each adhesion's dominant angle. We rotated each adhesion's frame of reference to match that adhesion's dominant angle and measured the mean absolute value difference between the adhesion's first measured angle and the rest of the adhesion's angle measurements.

SUPPLEMENTAL FIGURE LEGENDS

Figure S1 (relates to Fig. 1):

S1A) Panel (i) shows representative blot of clones from p34-KDR experiment with some clones showing knockdown rescue (3G6) and others showing only knockdown (1B3). Tubulin (Tub) was blotted as a loading control. Panel (ii) shows immunofluorescent staining of p34-KDR cells.

S1B) Diagram of the lentiviral vector combining p34Arc or Arp2 shRNA expression with EGFP or mCherry (mChry) expression flanked by LoxP sites.

S1C) Flow chart of stable Arp2/3-depleted cell line generation.

Supplemental Figure S2 (relates to Fig. 2):

S2A) NS and 2xKD cells treated with vehicle (DMSO) or BLB (15 μM) were immunostained for endogenous vinculin (Vin) and F-actin (Scale bar: 10 μm). Note the disappearance of focal adhesions and the reorganization of actin stress fibers in both cell types.

S2B) (upper panel) Cell lysates from NS, 2xKD and Arp2-KDR cells treated with DMSO or BLB were blotted for phospho-myosin light chain (Ser19), total myosin light chain (MLC-20) and GAPDH; (lower panel) bar graph showing pMLC(Ser19) quantification from three independent experiments (normalized to GAPDH). Error bar: 95% confidence interval. No statistically significant differences were observed between the cell lines with either treatment, although BLB caused a significant increase in pMLC (Ser19) levels in all three lines.

S2C) Cell lysates from IA32, Rat2, HEK 293 and HeLa cells treated with DMSO or BLB were blotted for phospho-myosin light chain 2 (Ser19), total myosin light chain (MLC-20) and GAPDH. Consistent with observations from endothelial cells (Goeckeler et al., 2008), BLB treatment caused a significant increase in levels of pMLC (Ser19). This effect appears to reflect a feedback loop where reduction of contractility caused by the inhibition of myosin heavy chain activity by BLB induces a calcium-dependent MLCK activation. However, it is important to note that increased pMLC does not reflect increased cellular contractility in this case.

Supplemental Figure S3 (relates to Fig. 3):

S3A) Bar graphs showing the NS and 2xKD CP and FMI comparisons

S3B) Serum chemotaxis: In this experiment, p34-KD cells (1B3 clone in Fig. S1) and p34-KDR cells were analyzed for chemotaxis to fetal bovine serum (FBS). Panel (i) shows endpoint plots, panel (ii) shows distribution of turn angles and panel (iii) shows table of results for different concentrations of FBS. Numbers in parentheses for each entry are 95% confidence intervals. Panels (i) and (ii) were plotted from the 15% FBS data set.

S3C) Bar graphs showing the CP FMI comparison of Rat2 fibroblasts treated with CK-666 or CK-689

S3D) NS cells before and 15 min after PDGF stimulation

Supplemental Figure S4 (relates to Fig. 5):

S4A) (i) Graphs showing the NS and 2xKD CP FMI comparison in haptotaxis with indicated FN source concentrations. (ii) Graphs showing the NS and 2xKD CP FMI comparison in haptotaxis with indicated ECM. Error bars: 95% confidence intervals.

S4B) Graphs showing the CP FMI comparison of CK-666 or CK-689 treated Rat2 cells in haptotaxi. Error bars: 95% confidence intervals.

Supplemental Figure S5 (relates to Fig. 6):

S5A) TIRF image of an NS cell expressing GFP-Paxillin on a 100 µg/mL FN coated surface (bar = 10µm).

S5B) High-pass filter applied to the image in S4A.

S5C) Distribution of high-pass pixel intensities from the entire time-lapse image series in S5A. The red dotted line indicates the focal adhesion pixel rejection threshold of the mean plus two standard deviations.

S5D) Locations of focal adhesions as determined by applying the threshold determined in S4C to the high-pass filtered image in S4B and overlaying the result on the image in S5A. Each identified adhesion is outlined in yellow.

Figure S6 (relates to Fig. 7):

S6A) Focal adhesions were segmented via the method described in (Fig. S4) and filtered to exclude adhesions with a major to minor axis ratio of less than three as indicated by color coding. The angle of the major axis with the positive x-axis was measured and the adhesions angles throughout the time-lapse image set pooled.

S6B) Sample search through the potential reference angles to determine the FAAI. The angle data set is from the entire time-lapse of the movie pictured in S5A).

SUPPLEMENTAL MOVIES

Movie 1 (Related to Fig. 1). Arp2/3 microinjection rescue of 2xKD cell: DIC time-lapse imaging was performed with 1 min time interval for 60 min. First frame of movie was captured prior to injection. This movie corresponds to Fig. 1F.

Movie 2 (Related to Fig. 2). Filling the gap: An example of a 2xKD cell carrying-out “filling the gap” motility. Related to Figure 2G. Phase contrast time-lapse imaging was performed with 10 sec time interval for 10 min.

Movie 3 (Related to Fig. 3). Chemotaxis: An example of a mixed population of NS (marked by GFP expression) and 2xKD cells migrating up a PDGF (80 ng/mL source concentration) gradient in the cell culture chamber. Related to Figure 3. TRITC-dextran labeled indicated the maintenance of the gradient. Epi-fluorescent and DIC time-lapse imaging were performed with 10 min time interval for 12 hr.

Movie 4 (Related to Fig. 3). Filopodia formation in 2xKD cells upon PDGF stimulation: An example of a serum-starved 2xKD cell after PDGF stimulation. DIC time-lapse imaging were performed with 15 sec time interval for 15 min.

Movie 5 (Related to Fig. 5). Haptotaxis: An example of a mixed population of NS (marked by GFP expression) and 2xKD cells migrating up a FN (150 μg/mL source concentration) gradient in the cell culture chamber. Only first frame of movie shows GFP image. Related to Figure 5. Phase contrast time-lapse imaging was performed with 10 min time interval for 5.5 hr.

Movie 6 (Related to Fig. 7). High and low FAAI cells: Examples of a low FAAI cell (left) and a high FAAI cell (right) expressing GFP-Pax. Adhesions with major/minor axis ratios of 3 or greater are color-coded in green, while those below this value are color-coded red. Related to Figure 7. TIRF imaging was performed with 150 sec time interval for 3 hr.

SUPPLEMENTAL REFERENCES

Bear, J., Loureiro, J., Libova, I., Fassler, R., Wehland, J., and Gertler, F. (2000). Negative regulation of fibroblast motility by Ena/VASP proteins. Cell *101*, 717-728.

Bear, J.E., Svitkina, T.M., Krause, M., Schafer, D.A., Loureiro, J.J., Strasser, G.A., Maly, I.V., Chaga, O.Y., Cooper, J.A., Borisy, G.G.*, et al.* (2002). Antagonism between Ena/VASP Proteins and Actin Filament Capping Regulates Fibroblast Motility. Cell *109*, 509-521.

Berginski, M.E., Vitriol, E.A., Hahn, K.M., and Gomez, S.M. (2011). High-resolution quantification of focal adhesion spatiotemporal dynamics in living cells. PLoS ONE *6*, e22025.

Cai, L., Makhov, A.M., Schafer, D.A., and Bear, J.E. (2008). Coronin 1B antagonizes cortactin and remodels Arp2/3-containing actin branches in lamellipodia. Cell *134*, 828-842.

Cai, L., Marshall, T.W., Uetrecht, A.C., Schafer, D.A., and Bear, J.E. (2007). Coronin 1B coordinates Arp2/3 complex and cofilin activities at the leading edge. Cell *128*, 915-929.

Goeckeler, Z.M., Bridgman, P.C., and Wysolmerski, R.B. (2008). Nonmuscle myosin II is responsible for maintaining endothelial cell basal tone and stress fiber integrity. American journal of physiology Cell physiology *295*, C994-1006.

Isaji, T., Sato, Y., Fukuda, T., and Gu, J. (2009). N-glycosylation of the I-like domain of beta1 integrin is essential for beta1 integrin expression and biological function: identification of the minimal N-glycosylation requirement for alpha5beta1. The Journal of biological chemistry *284*, 12207-12216.

Katsumoto, T., Naguro, T., Iino, A., and Takagi, A. (1981). The effect of tannic acid on the preservation of tissue culture cells for scanning electron microscopy. J Electron Microsc (Tokyo) *30*, 177-182.

Ozgur, S., Damania, B., and Griffith, J. (2011). The Kaposi's sarcoma-associated herpesvirus ORF6 DNA binding protein forms long DNA-free helical protein filaments. Journal of structural biology *174*, 37-43.

Svitkina, T.M.a.B., G. G. (2005). Correlative light and electron microscopy studies of cytoskeletal dynamics. Cell Biology: A Laboratory Handbook (Ed J Celis) *v. 3*, 277-286.

Supplemental Figure 1

Fig. S1

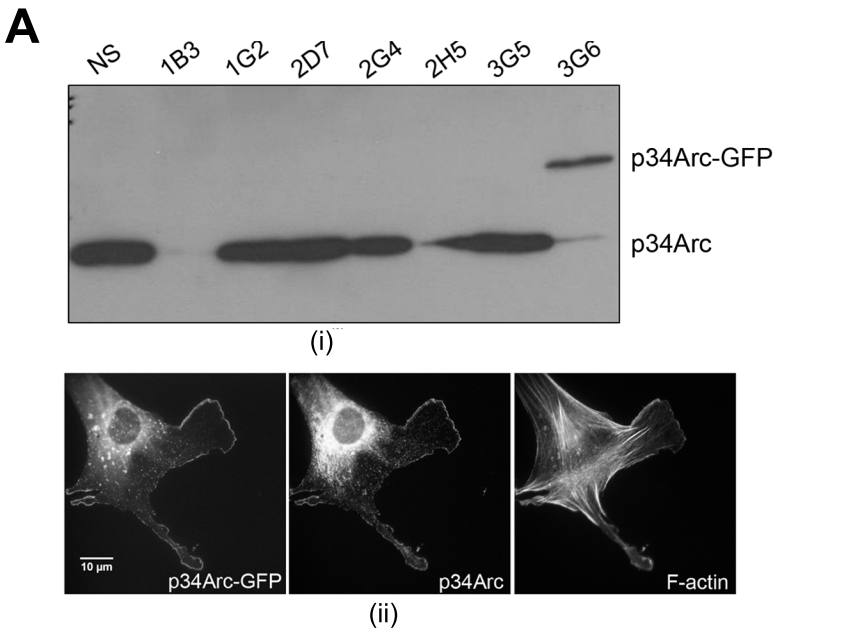

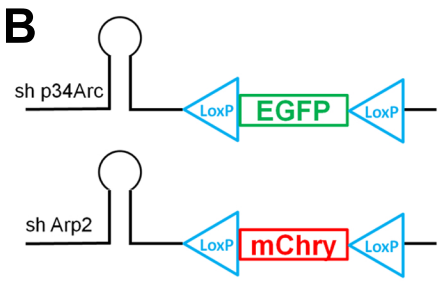

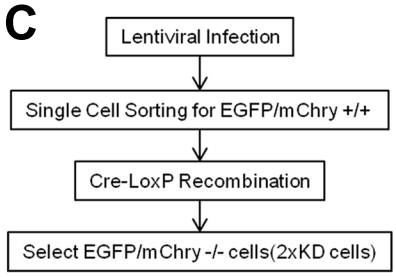

Supplemental Figure 2

Fig. S2

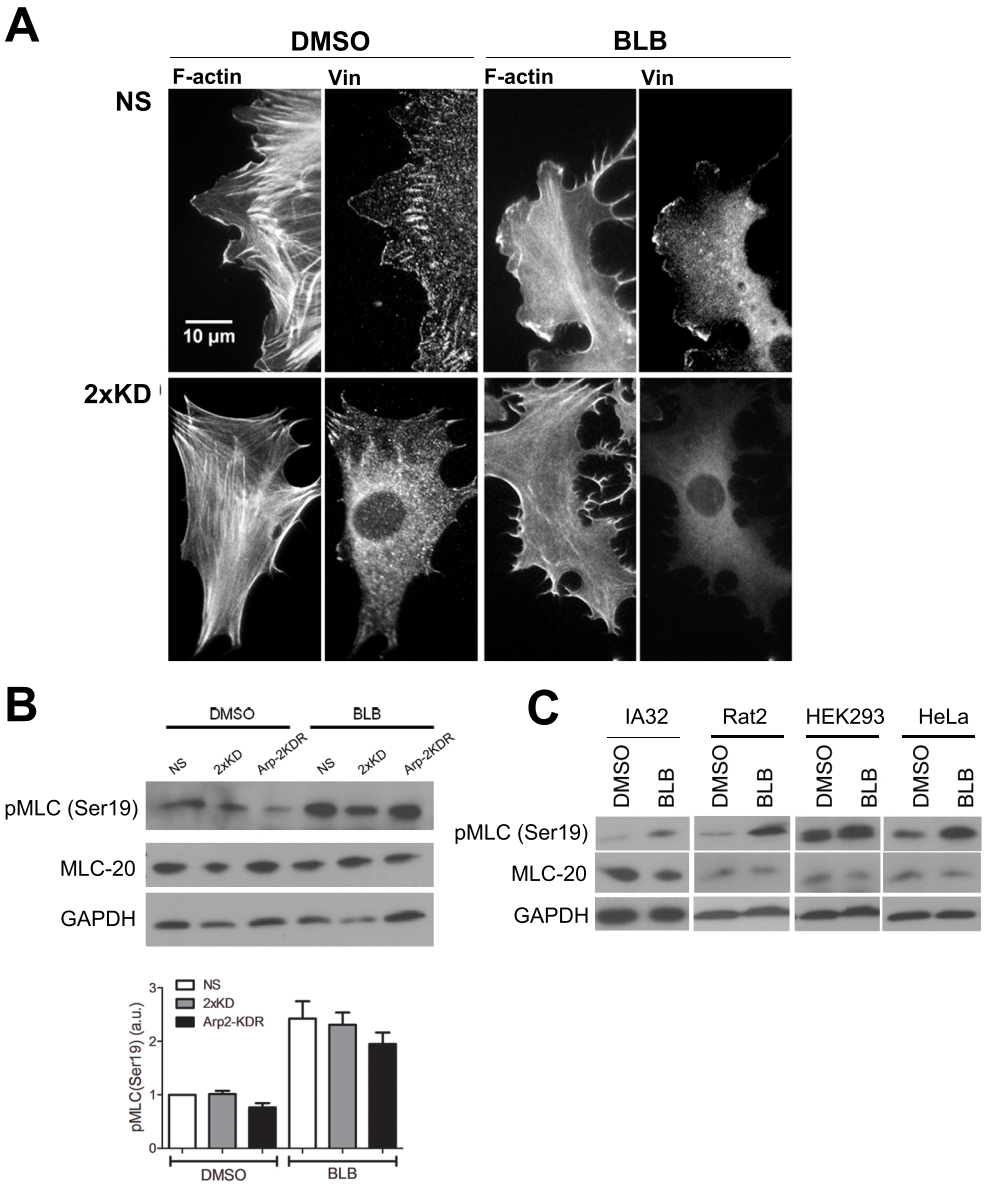

Supplemental Figure 3

Fig. S3

A

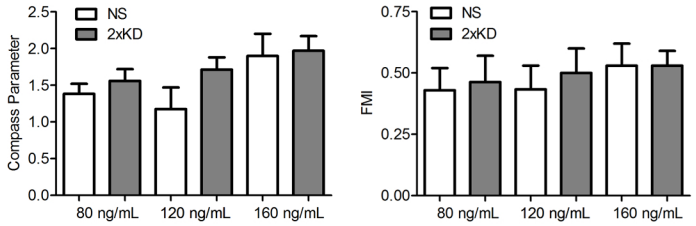

B

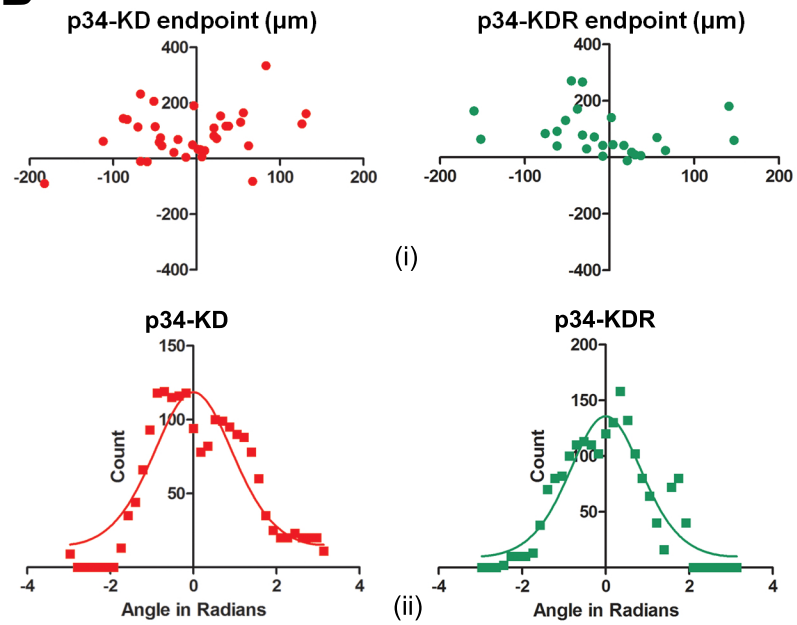

		10% FBS	12.5% FBS	15% FBS
p34-KD	CP	1.33 (1.12,1.55)	1.3 (0.63,2.01)	1.03 (0.77,1.3)
	FMI	0.33 (0.22,0.44)	0.57 (0.42,0.73)	0.35 (0.23,0.46)
p34-KDR	CP	1.11 (0.70,1.54)	1.90 (1.50,2.30)	1.01 (0.67,1.36)
	FMI	0.23 (0.11,0.34)	0.43 (0.33,0.52)	0.40 (0.31,0.50)

(iii)

C

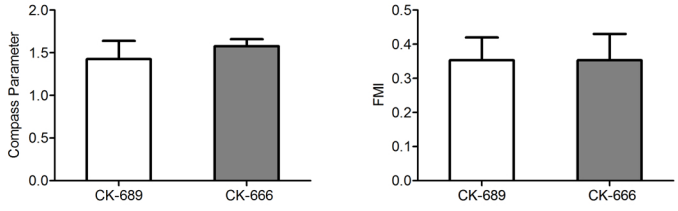

D

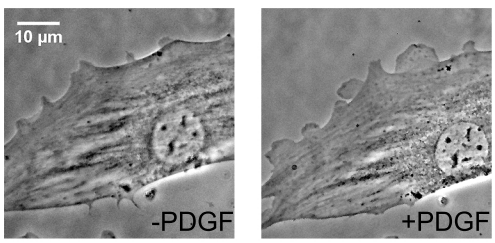

Supplemental Figure 4

Click here to download Supplemental Figure: 11-15-2011 FigS4.pdf

Fig. S4

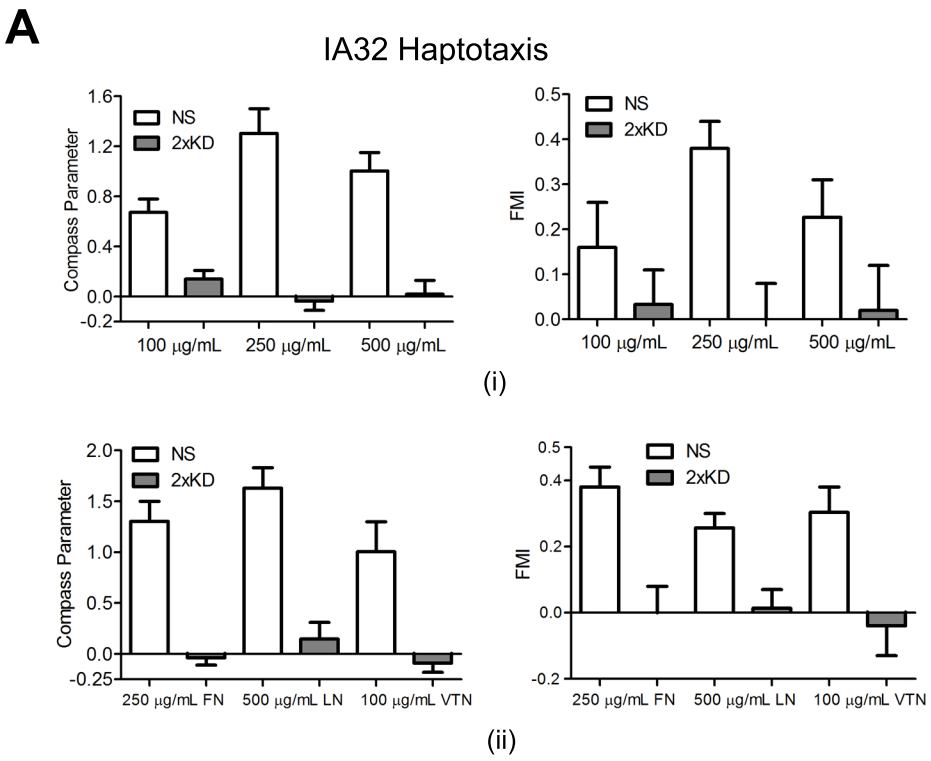

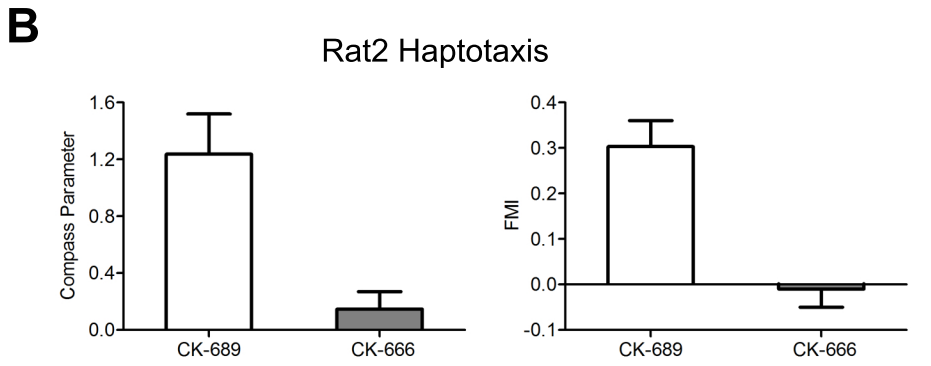

Supplemental Figure 5

Fig. S5

A

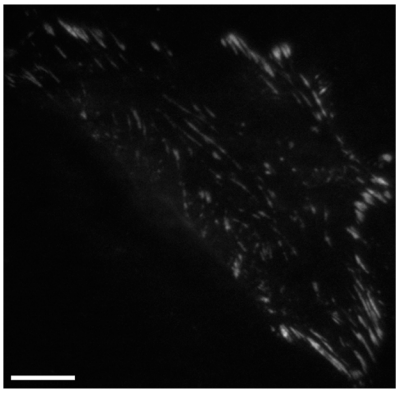

B

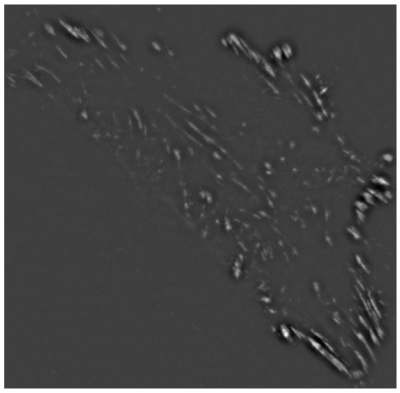

C

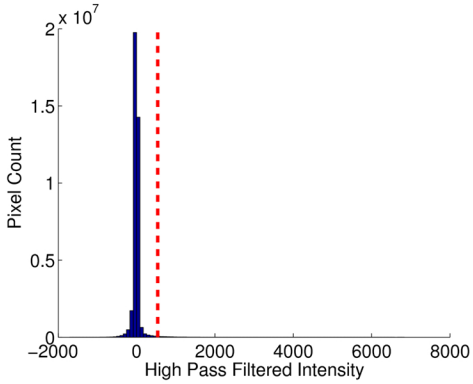

D

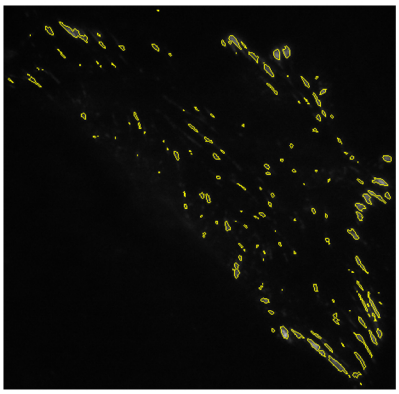

Supplemental Figure 6

Fig. S6